FISEVIER

Contents lists available at ScienceDirect

Acta Materialia

journal homepage: www.elsevier.com/locate/actamat



Full length article

Revisiting the Makishima–Mackenzie model for predicting the young's modulus of oxide glasses



Ying Shi^{a,*}, Adama Tandia^a, Binghui Deng^a, Stephen R. Elliott^b, Mathieu Bauchy^c

- ^a Science and Technology Division, Corning Incorporated, Corning, NY 14831, United States
- ^b Department of Chemistry, University of Cambridge, Lensfield Road, Cambridge CB2 1EW, United Kingdom
- ^c Physics of AmoRphous and Inorganic Solids Laboratory (PARISlab), Department of Civil and Environmental Engineering, University of California, Los Angeles, CA 90095, United States

ARTICLE INFO

Article History: Received 1 April 2020 Revised 15 May 2020 Accepted 20 May 2020 Available online 27 May 2020

Keywords: Young's modulus of oxide glass Makishima-mackenzie model Rigid unit packing fraction Dissociation energy The theoretically-derived Makishima-Mackenzie (MM) model expresses the Young's modulus of glass in terms of two determining factors, namely, the inter-atomic bonding strength (dissociation energy) and the ways in which atoms are packed (atomic packing fraction). This simple model offers a clear physical picture to understand the compositional dependence of the stiffness of glasses, but it generally underestimates the actual Young's modulus for many glasses, especially in the high value range. In this study, we argue that the inadequacy of the MM model mainly arises from its definition of the atomic packing fraction-which is defined as the ratio between the volumes of the atoms and the actual macroscopic volume of the glass. Such a definition results in a considerable amount of spacing within the basic building units being counted as free volume, which eventually leads to low packing fractions and, consequently, to low Young's modulus values. Here, we propose a more suitable packing metric, the Rigid Unit Packing Fraction (RUPF), which defines the basic building units as fully-filled, whole polyhedra made of "touching" oxygen atoms with no interstitial free volume. Young's moduli of 155 oxide glasses predicted from our revised MM model show a significantly improved level of agreement with respect to experimental data as compared to the original MM model. This study not only improves the ability of the physics-based MM model to yield accurate predictions of the Young's modulus, but also supports the relevance of rigid-unit theory, which could be applied as a basis to decipher other property-structure correlations.

 $\hbox{@ 2020 Acta Materialia Inc. Published by Elsevier Ltd. All rights reserved.}$

1. Introduction

The Young's modulus (e.g. of a silicate glass) defines its ability to withstand changes in length under length-wise tension or compression in the linear elasticity regime. As such, it is a critical engineering property for a large range of applications [1]. Understanding and predicting the compositional dependence of Young's modulus is therefore key to accelerating the discovery of novel glasses with tailored strength. Up to now, it has been studied extensively by physics-based models [2–5] and empirical data-based machine-learning (ML) models [6,7]. In particular, the Makishima-Mackenzie (MM) model [2], derived theoretically from the electrostatic attraction energy of ionic crystals, is described by a simple yet elegant equation shown as Eq. (1) in the original paper:

$$E = 2V_t \sum_i G_i X_i \tag{1}$$

where E is the Young's modulus (with a unit of GPa, which is also equivalent to kI/cm^3 , that is, a unit of energy per unit volume), V_t is

E-mail address: shiy3@corning.com (Y. Shi).

the atomic packing fraction (*APF*, defined in the conventional way as the ratio between the total volumes summed over all atoms and the actual volume calculated from measured mass density and composition), G_i is the dissociation energy per unit volume of the oxide component i, and X_i are the oxide mole fractions. However, it has been found that the MM model often under-estimates the actual Young's modulus for many glasses. The failure of the MM model has been attributed to the fact that it uses a macro-scale atomic packing density without incorporating any information regarding the network connectivity [8]. Therefore, topological constraint theory (TCT) has been adopted to account for the structural effect [4,5]. However, the network topology is not always accurately known, which makes it challenging to systematically apply TCT.

Molecular-dynamics (MD) simulation is also a commonly used physics-based method to compute the Young's modulus by applying a stress and calculating the resulting strain in a previously well-equilibrated simulation cell [3], or by applying a displacement-controlled load, and then measuring the derived stress as a result of the strain [9], or from the curvature of the potential-energy well [4]. The accuracy of MD simulations largely depends on the accuracy of the simulated glass structure that relies heavily on the accuracy of the underlying interatomic potentials, which is not always fulfilled. An

^{*} Corresponding author.

alternative approach is the data-driven, empirical machine-learning (ML) modeling technique [6,7]. ML is not only a data-driven solution but also a data-driven discovery tool that enables scientific predictions from incomplete models and incomplete data [10–12]. ML models rely on assessing a large number of data points to try to capture the hidden correlation between the input features and the output targets. However, if such hidden "physics laws" can be revealed and used as input constraints for an ML model, the accuracy and efficiency of model prediction can be dramatically improved.

In this study, we revisit the MM model by analyzing the two determining factors for calculating the Young's modulus: 1) APF; and 2) dissociation energy (DE) per unit volume. We find inadequacies in the definitions of both parameters. Firstly, we argue that, in contrast to the original MM model, the glass' total DE per unit volume should not be expressed as a simple summation of its individual oxide components' mole-fraction weighted DEs per unit volume. Volume-based energies are usually not additive parameters; rather, the additive rule may apply to mole-based energies, as demonstrated in Ref. [13,14]. Secondly, the conventional way to calculate the APF leads to low packing-fraction values. For example, the volume of a basic structural building unit, such as an SiO₄ tetrahedron, is defined by summing the volumes of one silicon and four oxygen individual atoms. Such a calculation leads to a considerable amount of free space within the tetrahedron being counted as free volume. This contravenes the "Rigid-Unit" theory, which suggests that the basic building units of a network glass should be treated as whole entities, and that their internal space should not affect the macroscopic response of a glass under loading. Instead, we herein propose a new packing-fraction metric, namely, the Rigid-Unit Packing Fraction (RUPF), which defines network-former building units as rigid and fully-filled polytopes made of "touching" oxygen atoms—a concept adopted from the oxygen-atom packing fraction [15,16]. In particular, this metric considers the interstitial space within the "touching" oxygen atoms as being fully filled (i.e., not as a free space). The Young's modulus values of 155 oxide glasses covering a wide variety of compositional ranges and Young's modulus values (from 15 to 140 GPa) have been calculated by the revised MM-model using the RUPF and subsequently calculated DE-values as the input. We demonstrate that our model offers significantly improved predictions of the Young's modulus as compared to other existing models. Furthermore, this study not only improves the ability of the physics-based MM model to yield accurate predictions of Young's modulus, but also supports rigid-unit theory which could be applied as a basis to decipher other property-structure correlations.

2. Studied glass groups

In this study, we focus on oxide glasses comprised of three common network-forming species, boron, silicon and aluminum. Unlike silicon with only one SiO₄ tetrahedral coordination, boron exists in BO₃ triangular and BO₄ tetrahedral coordination configurations,

aluminum has higher coordinated AlO_5 and AlO_6 configurations besides normal AlO_4 coordination. Boron and aluminum coordination numbers can be quantified by nuclear magnetic resonance (NMR), as shown for the calcium aluminoborosilicate (Ca-ABS) glasses [17]. The boron coordination number can also be directly calculated from the glass composition using the classic Yun and Bray model [18], as applied to sodium borate (Na-B) and sodium borosilicate (Na-BS) glasses [19] in this study. For the rest of the aluminosilicate glasses, we also assume that all the aluminum atoms possess a four-coordinated AlO_4 tetrahedral structure. This is an approximation because NMR measurements of calcium aluminosilicate glasses showed that the $^{\rm V}Al$ content per total Al is less than 5% for the percalcic region (where R < 0.5, and $R = C_{Al}/(2C_{Ca} + C_{Al})$, with C_{Al} and C_{Ca} being the elemental mol%), but it is up to 12% for the peraluminous region (where R > 0.5) [20].

The validity of the MM model relies on the accuracy of three pieces of experimental information: composition, density and Young's modulus. Data for a total of 155 oxide glasses were collected from the literature and 80 of those have experimentally measured composition data. The rest of the 75 glasses (which only present batch compositions) are still used because they cover different composition groups and significantly expand the range of Young's modulus values, namely, from 15 to 140 GPa—such as binary silicate glasses [21–23], binary borate glasses [19], ternary borosilicate glasses [19] and binary modifier-free aluminosilicate glasses [24]. The 155 glasses are categorized into eight groups in terms of compositions, with detailed information shown in Table 1.

3. Results

3.1. Young's modulus calculated by the original MM-definition (APF with volume summation DE)

First, the *E* values of 155 glasses were calculated using the MM model (Eq. (1)) with its original definition [2]. The atomic packing fraction (*APF*) is defined in the conventional way as being the ratio between the total volume summed over all atoms and the actual volume calculated from measured mass density and composition. The *APF* can be calculated by summing the volumes of all elements using Eq. (2):

$$\eta_{APF} = \rho \times \sum V_i C_i \tag{2}$$

where V_i is the volume of element i, which is calculated by $V_i = \frac{4}{3} \times \pi \times r_i^3$ with r_i being the Pauling effective ionic radii as listed in Table 2, the same values as used in the original MM model [2], C_i is the elemental mole fraction. ρ is the total atomic number density, which is calculated by $\rho = 0.6022 \times \rho_{mass} / \sum M_i C_i$, with ρ_{mass} being the measured mass density (g/cm³), and $\sum M_i C_i$ being the molecular weight of the glass, with M_i and C_i being the molar mass. The unit of E corresponds to energy per unit volume (kJ/cm³); therefore, the dissociation energy (DE) needs to have the same unit. The MM model

Table 1Composition information of eight glass groups with their network-former and modifier species, data size, compositional range of each individual oxide components.

Groups	Former	Modifier	Data size	Formula	Composition range (mol%)			
					x	у	100-x-y	
M-S [21] [23] [23]	Si	Li, Na, K, Ca, Sr, Ba	12	(R ₂ O/RO) _x (SiO ₂) _{100-x}	10-40		60-90	
AS [24]	Si, Al	None	7	$(Al_2O_3)_x(SiO_2)_{100-x}$	0 - 60		40 - 100	
Na-B [19]	В	Na	10	$(Na_2O)_x(B_2O_3)_{100-x}$	0 - 50		50-100	
Ca-AS ^[25]	Si, Al	Ca	26	$(CaO)_x(Al_2O_3)_v(SiO_2)_{100-x-v}$	12 - 34	10 - 34	33-77	
M-AS [22] [23] [26] [27]	Si, Al	Li, Na, K, Mg, Ca, Sr, Ba, Zn	31	$(R_2O/RO)_x(Al_2O_3)_v(SiO_2)_{100-x-v}$	20 - 42	5-25	40 - 76	
NaM-AS [28]	Si, Al	Na:M = 3.9:1 (M=Mg, Ca)	20	$(Na_2O)_{16}(MO)_8(Al_2O_3)_x(SiO_2)_{76-x}$	0 - 24			
Na-BS [19]	Si, B	Na	34	$(Na_2O)_x(B_2O_3)_y(SiO_2)_{100-x-y}$	3 - 40	13-50	30-80	
Ca-ABS [17]	Si, Al, B	Ca	15	$(CaO)_{15}(Al_2O_3)_{15}(B_2O_3)_x(SiO_2)_{70-x}$	5-25			

Table 2Parameters used for *APF* and *RUPF* calculations. I) *APF*: Pauling's effective ionic radii for O, network formers and modifiers corresponding to their specified coordination numbers; Whittaker-Muntus' ionic radii for O and network formers; individual polyhedral volume of formers defined by *APF*; II). *RUPF*: touching oxygen radius for network formers, modifier-oxygen bond length, modifier effective ionic-radius calculation corresponding to touching oxygen atoms; interstitial space packing fraction of polyhedra, individual polyhedral volume of formers defined by *RUPF*.

Network formers		E	В		Al				0
Coordi	Coordination number		4	4	4	5	6		
APF RUPF	Pauling's effective ionic radius (Å) ^{1 [29]} Whittaker-Muntus' ionic radius (Å) ^{1 [30]} Individual polyhedron volume (Å) Touching oxygen radius (Å) [15,16] Interstitial space packing fraction [31] Individual polyhedron volume (Å)	0.01 0.1 30.92 1.178 0.395 ² 25	0.11 0.2 41.23 1.207 0.26 32.03	0.26 0.34 41.3 1.306 0.26 40.6	0.39 0.47 41.47 1.437 0.26 54.09	0.48 0.56 51.99 1.334 0.368 ² 55.51	0.535 0.61 62.48 1.328 0.476 ² 67.79		1.35 1.27
	rk modifier nation number	Li 4	Na 6	К 9	Mg 5	Ca 6	Sr 7	Ba 8	Zn 5
APF RUPF	Pauling's effective ionic radius (Å) [²⁹] M-O bond length (Å) (r _{M-O} =r _M +r _O) Modifier ionic radius corresponding to touching oxygen(Å)	0.59 1.94 r _{M-O} -r _õ (1.02 2.37 r _õ -mean t	1.55 2.9 ouching o	0.66 2.01 oxygen rac	1.00 2.35 lius)	1.21 2.56	1.42 2.77	0.68 2.03

¹ The Pauling's effective radii [29] are used for *APF* calculation as they were used in the Makishima-Mackenzie (MM) model [2]; the Whittaker-Muntus values [30] were specially derived for silicate minerals; therefore, they are used for the 2D-schematic illustration of *APF* polyhedra of Fig. 4.

expresses the DE per unit volume (G_{glass}^V) via a summation of mole fraction weighted G_i^V over all the oxide components. In the original MM paper [2], two DE values $(G_i^{mole} \ and \ G_i^V)$ are listed for a series of oxides. The G_i^{mole} value is the same as that originally determined by Sun and Huggins [13,14]. The G_i^V value is claimed to be back-calculated from the pure oxide E value using Eq. (1). However, the calculation method of these values is not fully detailed. Later, the G_i^V values have been mathematically amended by other MM model users in order to improve the accuracy of the E prediction [22,23]; unfortunately, no justifications were provided in terms of how the new G_i^V values were derived. Here, the original G_i^V values from the MM paper are listed in Table 3 as the reference.

As defined in Eq. (1), the glass total DE per unit volume is calculated by $\sum G_i^V X_i$, where G_i^V is each oxide DE per unit volume (kJ/cm³), as listed in Table 3, and X_i is the oxide mole fraction.

The calculated E values, derived using the original MM definition, are plotted against the measured E values for all 155 glasses in Fig. 1. Detailed information is provided in the Supplementary Data Tables S1 &2. With the intercept being fixed at zero, a linear fitting of calculated vs. measured values in Fig. 1 yields a slope of 0.866 with a root mean-squared error (RMSE) of 11.505 GPa. We observe that the MM model systematically under-estimates E, especially in the high-E region (E>80 GPa) for glasses containing Al₂O₃. Such an under-estimation is also shown in the original MM-paper [2] and has often been reported by others [4,22,23]. The correlation between calculated and measured values is fair for the binary sodium borate glasses in the low-E region (E< 60 GPa). It is especially good for the pure B₂O₃ glass, with a calculated value of 16.13 GPa in comparison to the measured value of 17 GPa [2]. Our result contrasts with the calculated value of 62 GPa obtained by Zwanziger et al. in Ref. [8], wherein the

Table 3Dissociation energy derived from different sources as well as the modifier cation field strength.

Network former		SiO ₂ ¹		$Al_2O_3^2$			$B_2O_3^{3}$			
		SiO	94	AlO ₄	Ald	06	BO ₃	E	BO ₄	
G_i^V (kJ/cm ³) G_i^{mole} (kJ/mol)	MM [2] Original Sun-Huggins ^[13] RUPF-derived APF-derived	64. 1774 – 1744(1879(1950 (21)	133.9 2653 3247(55) 4730(60)	N. 33 7592(7520(64 (989)	16.3 682 655(50) 575(54)	29 3382	77.8 2979 3382(121) 3280(131)	
Network modi	fier	Li ₂ O	Na ₂ O	K ₂ O	MgO	CaO	SrO	BaO	ZnO	
G_i^V (kJ/cm3)	MM ^[2]	80.3	37.2	23.4	83.7	64.9	48.5	40.6	41.4	
G_i^{mole} (kJ/mol)	Original Sun-Huggins [13]	1205	1004	962	929	1075	1071	1088	602	
	RUPF-derived APF-derived	1372(129) 1335(140)	962(60) 836(65)	493(190) 227(207)	1402(178) 1399(194)	1389(72) 1364(78)	1263(142) 1172(155)	980(96) 843(105)	1471(313) 1575(341)	
Modifier's catio	in field strength ($Å^{-2}$)	2.87	0.96	0.42	4.59	2.00	1.37	0.99	4.33	

^{1.} Low G_i^{mole} value (1774 kJ/mol) corresponds to fully polymerized SiO₂, where all oxygen atoms are bridging; high G_i^{mole} value (1950 kJ/mol) corresponds to total depolymerized Ca₂SiO₄, where all the oxygen atoms are non-bridging. The low G_i^{mole} value (1774 kJ/mol) shown as bold was listed in the MM paper [2].

 $^{^2}$ The interstitial packing fraction of BO₃, AlO₅ and AlO₆ polyhedra is defined in the Supporting Information section.

^{2.} Low G_i^{mole} value (2653 kJ/mol) corresponds to aluminosilicate material with AlO₄ coordination; the high G_i^{mole} value (3364 kJ/mol) corresponds to aluminate material with AlO₆ coordination. The high G_i^{mole} value (3364 kJ/mol) shown as bold was listed in the MM paper [2] although the MM paper did not specify Al-O coordination numbers.

^{3.} The Sun-Huggins paper [13] only listed one G_i^{mole} value (2979 kJ/mol) for borate, corresponding to BO₄ coordination, while the MM paper [2] calculated the G_i^V value (16.3 kJ/cm3) of BO₃ coordination from the E value of pure B₂O₃ glass which contains entirely BO₃ triangular configurations. Therefore the G_i^{mole} value (682 kJ/mol) for BO₃ coordination is calculated from the G_i^V value and mole volume of B₂O₃ glass and used for the molar summation of DE calculation.

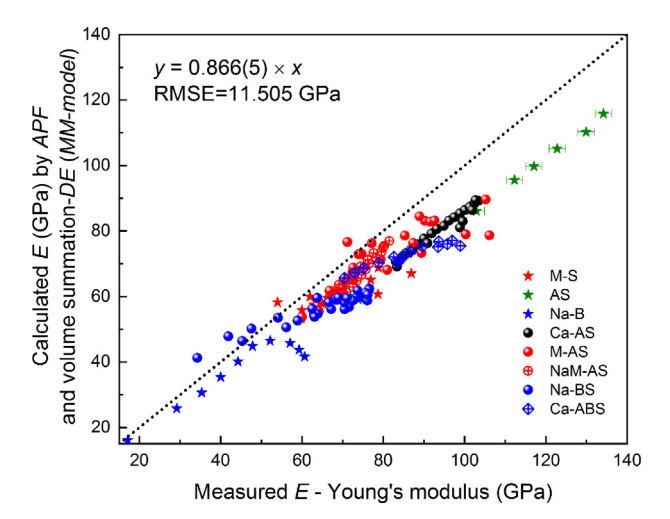


Fig. 1. Relationship between calculated and measured values of the Young's modulus of 155 glasses, where the calculated value is derived using the original MM definition, with APF and DE values calculated by unit volume summation. The dotted line y = x represents the ideal correlation. The slope derived by linear fitting with the intercept fixed as zero, is 0.866, indicating under-estimation by the MM-model, with an RMSE of 11.505 GPa. The error bars of measured E values were reported for 87 glasses; only seven AS glasses have error bars (± 1 GPa) larger than the symbol size.

discrepancy between calculated (62 GPa) and measured (17 GPa) Young's modulus values was attributed to the fact that the Young's modulus should vanish to zero in isostatic or under constrained glasses. However, we argue that their high calculated value of 62 GPa is mainly caused by using the wrong dissociation energy (namely, 77.8 kJ/cm³ for BO₄ units). Rather, we propose that the *DE* value of 16.3 kJ/cm³ (Table 3) should be used for BO₃ triangular units—since pure B₂O₃ glass solely contains BO₃ triangular units.

3.2. Young's modulus calculated by APF with molar summation DE

We argue that the glass' total volumetric DE should not be expressed as a simple weighted summation of the oxide components' volumetric DEs. Volume itself, and all volume-based properties, are not always additive parameters; the additive rule might apply to mass or mole-based properties, as stated clearly in the very first two papers introducing the concept of glass dissociation energy [13,14]. The volume-summation DE calculation method used in the MM paper [2] was also adopted by others [22,23]. A more accurate way to calculate the DE per unit volume of a glass is shown in Eq. (3), which takes the form of a weighted sum of the total molar DE values of all the oxide components $(G_i^{mole}X_i)$ divided by the glass' molar volume $V_{\rm m}$, which is calculated from the glass' composition and density:

$$DE_{per\ unit\ volume} = \frac{\sum G_{i}^{mole} X_{i}}{V_{vo}} \tag{3}$$

where G_i^{mole} is the DE per mole for oxide component i, which was calculated by Sun and Huggins [13,14] and listed in Table 3, X_i is the oxide mole fraction. $V_{\rm m}$ is the glass' molar volume and calculated by $V_m = \frac{\sum_{i=1}^{M_i X_i}}{\rho_{\rm mass}}$, with M_i and X_i being the molar mass and mole fraction of oxide i, and $\rho_{\rm mass}$ is the measured mass density (g/cm³). The same way of expressing the glass DE per unit volume as our definition is also reported in Ref. [32].

The correctness of molar summation can be further confirmed by a pressurization study of 15 calcium aluminoborosilicate (Ca-ABS) glasses, which are from five compositions $(CaO)_{15}(Al_2O_3)_{15}(B_2O_3)_x(-SiO_2)_{70-x}$ (x = 5, 10, 15, 20, 25), with each composition containing three glasses, as-made, 1 and 2 GPa hot-compressed [17]. After pressurization, both density and E increase; the coordination numbers of B and Al also increase, as shown by NMR measurements. As expected,

pressurization increases the packing fraction; it should also increase DE because the bond strength increases as the bond length decreases. However, the volumetric summation method $(\sum G_i^V X_i)$ only uses composition for the DE calculation; in contrast, the molar summation method takes account of the density change, which is represented by the molar volume V_m as shown in Eq. (3). The DE values calculated by both methods for 15 Ca-ABS glasses are plotted in Fig. 2. For each composition, the molar summation – derived DE increases significantly with pressure mainly due to the density increase. In contrast, the volumetric summation – derived DE increases slightly with pressure, due to the BO_4 fraction increase which has a much higher $G_{BO_4}^V$ value (77.8 kJ/cm³) compared to $G_{BO_3}^V$ (16.3 kJ/cm³), as listed in Table 3. Apparently, the molar-summation method produces DE values which better align with physics expectation – i.e. pressurization increases DE.

Fig. 3 shows the calculated E values derived by APF and molar-summation DE values plotted against the measured E values. We find that the correlation between calculated and experimental data does not improve for the DE calculated by the correct method, with an RMSE as high as 11.921 GPa. Compared to Fig. 1 with the calculated E values derived from the volumetric summation-DE, the data points are less scattered in Fig. 3, particularly by the lining up of 15 Ca-ABS glasses. But the deviation between calculated and measured E values systematically increases as the E-value increases, which is in turn correlated to an increase in the Al_2O_3 content. This leads us to investigate the role of the other determining factor, i.e., the packing fraction.

3.3. Young's modulus calculated by RUPF with correct DE

3.3.1. A suitable way to define packing fraction - RUPF

The whole volume of a network-glass structure is essentially composed of three packing elements: (i) network-forming building units; (ii) network-modifying ions (when present); and (iii) free volume. As stated above, the conventional *APF* definition under-estimates the packing fraction by generating considerable amounts of free space within the basic building units. Here, we propose a new packing-fraction metric, namely, the Rigid-Unit Packing Fraction (*RUPF*). This metric considers the basic network-forming building units to be "rigid" and fully filled (i.e., with no internal free space) [33]. To this end, we adopt the concept of "touching" oxygen spheres, which was first introduced by Wang et al. [15], and then applied to the oxygen-packing fraction (*OPF*) by Zeidler et al. [16]. An AO₄ (*A* = *B*, Si or Al) tetrahedron is used to demonstrate the difference between *APF* and *RUPF*. As

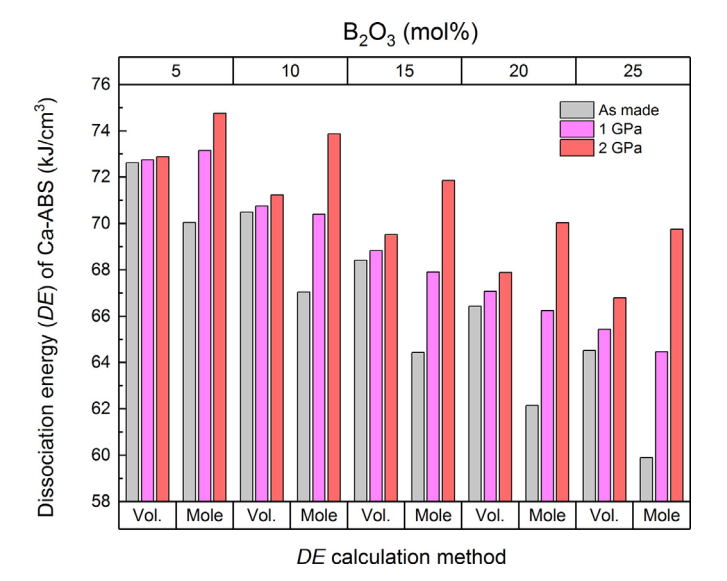


Fig. 2. Dissociation energy of 15 Ca-ABS glasses calculated by volumetric and molarsummation methods.

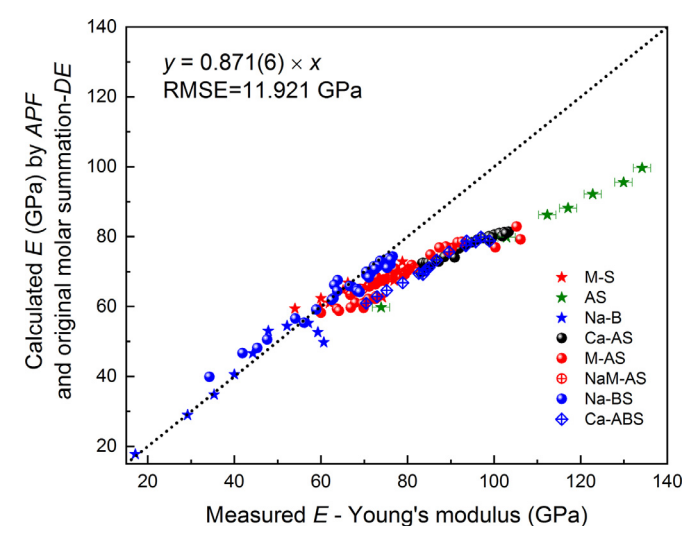


Fig. 3. Relationship between calculated and measured values of Young's modulus of 155 glasses, where the calculated value is derived using the original MM definition with *APF*, but with *DE* calculated by the correct molar summation. The dotted line y = x represents the ideal correlation. The slope derived by linear fitting, with the intercept fixed as zero, is 0.871, indicating under-estimation with an *RMSE* value of 11.921 GPa.

illustrated in Fig. 4(a), (b) & (c), in contrast to the conventional *APF* that defines a tetrahedron by four individual oxygen spheres surrounding a central network former as shown in Fig. 4(d), (e) & (f), the *OPF* defines an AO₄ tetrahedron as a polytope made of four touching oxygen spheres, with the radius $r_{O,A}$ (A = B, Si or Al) being scaled to the A-O bond length (r_{A-O}) by $r_{O,A} = \sqrt{2/3}r_{A-O}$.

The definition of touching oxygen spheres still leaves some empty interstitial space within the tetrahedron, shown as the pink shaded area in Fig. 4(a), (b) & (c). Its volume can be calculated using a knowledge of the packing density of close-packed monodisperse spheres, i. e., 0.74 [31] — since a tetrahedron formed by four touching atoms represents one basic building unit of close-packed spheres of equal radii. For close-packed spheres, each interstitial space is formed by four touching spheres, and each sphere is also surrounded by four

interstitial spaces. Therefore there are equal numbers of spheres and interstitial spaces. Since the volume fraction of the spheres is 0.74 and that of interstitial space is therefore 0.26, the interstitial volume can be calculated from the sphere volume with Eq. (4)

$$V_{interstitial} = \frac{0.26}{0.74} V_{sphere} = 0.351 V_{sphere} \tag{4}$$

where $V_{\rm sphere}$ is the touching-oxygen volume, which is calculated as $V_{\rm sphere}=4/3\pi r_{\rm O,A}^3$ with $r_{\rm O,A}$ as the touching-oxygen radius (A = B, Si or Al).

Therefore, the total volume of an AO₄ tetrahedron defined by RUPF is 4.351 times the one touching oxygen volume, that is, the sum of the volumes of four touching oxygen atoms and that of the interstitial space. The individual AO₄ tetrahedral volumes of B, Si and Al are calculated using both APF and RUPF methods and listed in Table 2. The three APF volumes calculated from Pauling's effective ionic radii are 41.23, 41.3 & 41.47 Å³ for B, Si and Al-tetrahedra, respectively. Using B and BO₄ as reference, the ionic radii of Si and Al increase by 1.36 and 2.55 times, but their corresponding tetrahedral volumes only increase by 0.16 and 0.59% relatively. This is because, by the APF definition using Pauling's atomic radii, more than 99% of the AO₄ volume is from four oxygen atoms, with less than 1% volume contributed by the network-former atom. Such a network-former insensitivity reflects that the APF definition does not capture the true glass-packing physics. On the contrary, the three RUPF volumes calculated from touching oxygen radii are 32.03, 40.6 & 54.09 Å³ for B, Si and Al-tetrahedra, respectively. The two methods produce quite similar values for an SiO₄ tetrahedron, with the RUPF volume of 40.60 Å³ and the APF volume of 41.30 Å^3 . The difference is more noticeable for the smaller BO₄ tetrahedron, where the RUPF method gives a volume of 32.03 $Å^3$, in comparison to the value of 41.23 $Å^3$ obtained by the APF method. In contrast, the difference between RUPF and APF values for the larger AlO₄ tetrahedron is opposite, where the RUPF method gives a larger volume of 54.08 Å³, in comparison to the APF value of 41.47 Å³. In other words, the *RUPF* method is essentially equivalent to considering network-forming polytopes as being fully filled, and adjusting the effective radius of oxygen atoms until they eventually touch each other. This correction becomes even more pronounced when the central cation is small enough to "pull" the oxygen neighbors

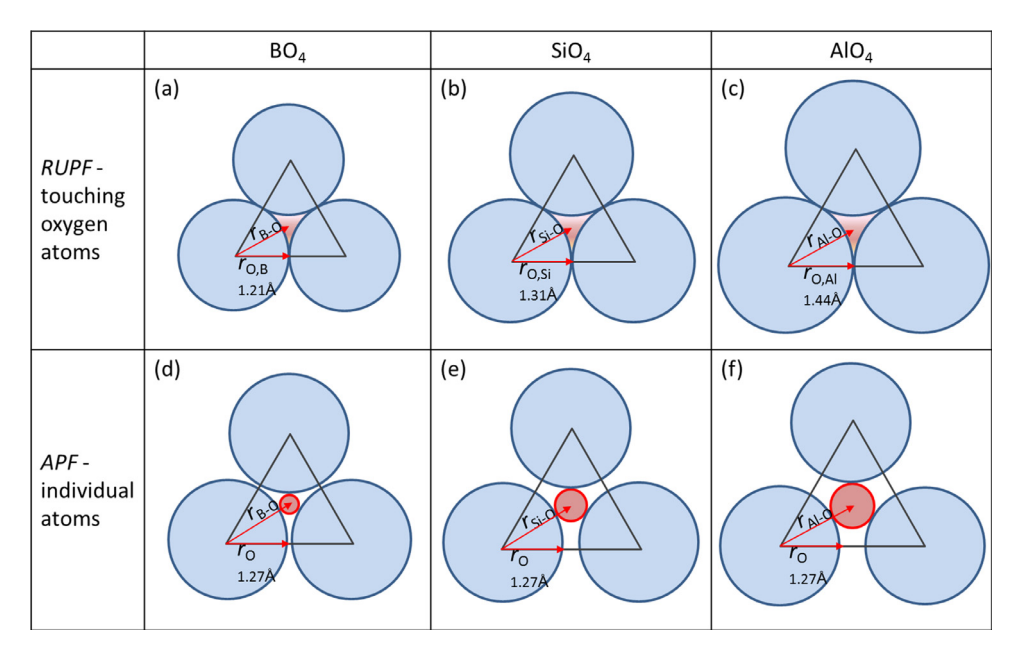


Fig. 4. 2D-schematic illustration of RUPF (a, b & c) and APF (d, e & f) for BO_4 , SiO_4 and AlO_4 tetrahedra. The Rigid-Unit packing fraction (RUPF) defines the tetrahedron by four touching oxygen spheres, whose radius r_{OA} (A = B, Si or Al) is scaled to the A-O bond length (r_{A-O}) by $r_{OA} = \sqrt{2/3}r_{A-O}$ and the pink shaded area is the interstitial space. The conventional atomic packing fraction (APF) used in the MM-model [2] defines a tetrahedron as four individual oxygen spheres surrounding the central network former (B, Si or Al). The APF schematic is drawn using the Whittaker-Muntus' radii [30], as listed in Table 2.

close to each other (e.g., as in the case of B atoms), or large enough to "push" the oxygen neighbors far away from each other (e.g., as in the case of Al atoms). The difference between the two methods can be clearly demonstrated in the 2D schematic illustration in Fig. 4, where no clear difference can be seen for the *APF* plots (d-f) of three tetrahedra, while the *RUPF* plots (a-c) show a visible volume increase in the order of BO₄, SiO₄ and AlO₄.

3.3.2. Rigid-Unit packing fraction (RUPF) calculation

As illustrated above, the total *RUPF* packing fraction is calculated by adding the three components using Eq. (5):

$$\eta_{RUPF} = \eta_{O} + \eta_{interstitial} + \eta_{M} \tag{5}$$

where η_O is the total touching oxygen packing fraction, $\eta_{interstitial}$ is the total interstitial empty space within tetrahedra, and η_M is the total modifier packing fraction.

First, the calculation procedure for η_0 reported in Ref. [16] is summarized below. η_0 is defined in Eq. (6):

$$\eta_0 = V_0 \rho_0 \tag{6}$$

where ρ_O is the oxygen number density, which is further defined as $\rho_O = \rho \times C_O$, with ρ being the measured total atomic number density and C_O the atomic fraction of oxygen atoms. For an oxide glass with n-fold coordinated network formers B (n = 3 and 4), Si (n = 4) and Al (n = 4, 5 and 6), V_O is the mean oxide-ion volume of mixed AO₄ polyhedra, and is defined by Eq. (7):

$$V_{O} = \frac{4}{3}\pi \frac{\sum_{n=3}^{4} n \times C_{B^{[n]}} r_{O,B^{[n]}}^{3} + 4 \times C_{S^{[4]}} r_{O,S^{[4]}}^{3} + \sum_{n=4}^{6} n \times C_{A^{[n]}} r_{O,A^{[n]}}^{3}}{\sum_{n=3}^{4} n \times C_{B^{[n]}} + 4 \times C_{S^{[4]}} + \sum_{n=4}^{6} n \times C_{A^{[n]}}}$$
(7)

where $C_{A^{[n]}}$ is the atomic fraction of network former A with n-coordination, which can either be measured by NMR (for B and Al) or calculated from composition (for B only). The radius of touching oxygen atoms ($r_{O,A^{[n]}}$) is the effective oxide-ion sizes scaled by the corresponding AO_n polyhedron size.

The touching oxygen radius $r_{O,A^{[4]}}$ of an AO₄ tetrahedron can be calculated by Eq. (8):

$$r_{OA^{[4]}} = \sqrt{2/3} r_{A^{[4]} - O} \tag{8}$$

where $r_{A^{[4]}\!-\!O}$ is the experimental measured A-O bond length for AO₄ coordination; $r_{O,B^{[4]}}$ is 1.207 Å for $r_{B^{[4]}\!-\!O}\approx 1.478$ Å, $r_{O,S^{[4]}}$ is 1.306 Å for $r_{S^{[4]}\!-\!O}\approx 1.60$ Å and $r_{O,A^{[4]}}$ is 1.437 Å for $r_{A^{[4]}\!-\!O}\approx 1.76$ Å, as listed in Table 2.

The concept of using "touching" oxygen atoms was further extended to other network-forming building-unit motifs by Zeidler et al. [16], such as planar BO₃ triangles and AlO₅ and AlO₆ polyhedra; their corresponding "touching" oxygen radii are also listed in Table 2.

Next, the interstitial space within tetrahedra, $\eta_{\text{interstitial}}$, is calculated by Eq. (9):

$$\eta_{interstitial} = \sum_{n=3}^{6} \frac{\eta_{interstitial}^{AO_n}}{1 - \eta_{interstitial}^{AO_n}} \times \rho \times \frac{3}{4}\pi \times C_{A^{[n]}} r_{O,A^{[n]}}^{3}$$
(9)

with $\eta_{interstitial}^{AO_n}$ being the interstitial-space packing fraction of AO_n polyhedra and all the parameters are defined as above. As described in the previous section, the value of $\eta_{interstitial}^{AO_a}$ is 0.26. The other $\eta_{interstitial}^{AO_n}$ values for AO₃, AO₅ and AO₆ polyhedra are defined in Supporting Information and listed in Table 2.

Similarly, the modifier ion-packing fraction, η_M , is calculated by Eq. (10):

$$\eta_{M} = V_{M} \rho_{M} \tag{10}$$

where ρ_M is the modifier number density defined in the same way as ρ_O , and V_M is the modifier-ion volume defined as $V_M = (\frac{4}{3})\pi r_M^3$. r_M is the atomic radius of M, which varies with the modifier coordination number. The coordination number [16] and its corresponding Pauling

effective ionic radii [29] used in the MM-model are listed in Table 2. The Pauling effective ionic radii [29] or other forms of radii, such as Whittaker-Muntus radii [30] (also called crystal radii), are compiled from experimentally measured bond-length values by assuming a reference value for oxygen anions (1.35 Å for Pauling effective oxygen radii and 1.27 Å for Whittaker-Muntus radii). Therefore, the M-O bond lengths are calculated by summing the oxygen and modifier radii, and are listed in Table 2. In the RUPF calculation, the oxygen radii are adjusted until touching to form AOn polyhedra; consequently, the modifier radius should be adjusted accordingly to keep the M-O bond length constant and to avoid over or under-counting the packing fraction. The value of $r_{\rm M}$ is calculated by Eq. (11):

$$r_{\rm M} = r_{\rm M-O} - r_{\rm O} \tag{11}$$

where r_{M-O} are the M-O bond lengths calculated from the sum of oxygen and modifier radii and listed in Table 2, and r_O is the mean oxide-ion radius of mixed AO_n polyhedra, and is calculated by Eq. (12):

$$r_0 = \sqrt[3]{V_0 \times \frac{3}{4\pi}}$$
 (12)

where V_0 is the mean oxide-ion volume of mixed AO₄ polyhedra, and is defined by Eq. (7).

3.3.3. RUPF of 26 CAS glasses

A set of 26 calcium aluminosilicate (CAS) glasses [25] were used to compare the difference of new-RUPF and conventional APF values; the data are given in Supplementary Data Table S1. As shown in the compositional phase diagram of Fig. 5(a), there are three series for the 26 glasses: series I are charge-balanced glasses; series II and III are glasses with constant SiO₂ contents. In Fig. 5(b), the RUPF (solid balls) and APF (crossed balls) of series I glasses are shown with red color as a function of mol% of SiO₂, while series II and III' glasses are plotted with black and blue colors in Fig. 5(c) as a function of R-values, where $R = C_{AI}/(2C_{Ca} + C_{AI})$. As expected, the RUPF values for all the glasses are higher than their corresponding APF-values, the difference becoming more pronounced as the Al₂O₃ content increases because the rigid-unit volume of AlO₄ defined by RUPF is significantly larger than that by APF. For the constant SiO2-containing glasses in series II and III, as the R-value increases by more Al₂O₃ substituting for CaO, the glasses become more polymerized, which should lead to an increase in packing fraction. As shown in Fig. 5(c), both series show an increase in RUPF with R-value; in contrast, slight decreases are observed in the APF series, which does not reflect the true packing fraction.

To further illustrate the difference between RUPF and APF, the tetrahedral building unit $(\eta_{\rm A})$, modifier $(\eta_{\rm M})$ and total packing fraction as a function of R-value for series II and III glasses are plotted in Fig. 6. As the R-ratio increases, η_A^{RUPF} (solid symbols) increases significantly due to the significantly large AlO_4 volume by the RUPF definition, while η_A^{APF} (crossed symbols) only increases slightly with increasing Al content. Both η_M^{RUPF} and η_M^{APF} decrease as R increases because the number of modifier atoms decreases. For series III glasses, η_M^{RUPF} is significantly smaller than η_M^{APF} due to its smaller effective $r_{\rm M}$ deduced from the larger r_O by the high Al_2O_3 content in series III glasses. The total RUPF increases with R, but APF slightly decreases because of its under-estimation of the tetrahedral packing fraction.

3.3.4. Young's modulus calculated by RUPF with original correct DE

Fig. 7 shows the calculated E values obtained from the RUPF and molar summation DE using the original dissociation energy data from Sun [13,14], plotted against measured E values. The RMSE of the degree of correlation drops to 4.003 GPa, which is only about one third of the original MM model's RMSE value (11.505 GPa). Significant improvement occurs in the high E-region (E >60 GPa) with Al_2O_3 -containing glasses. Their calculated E-values increase by the

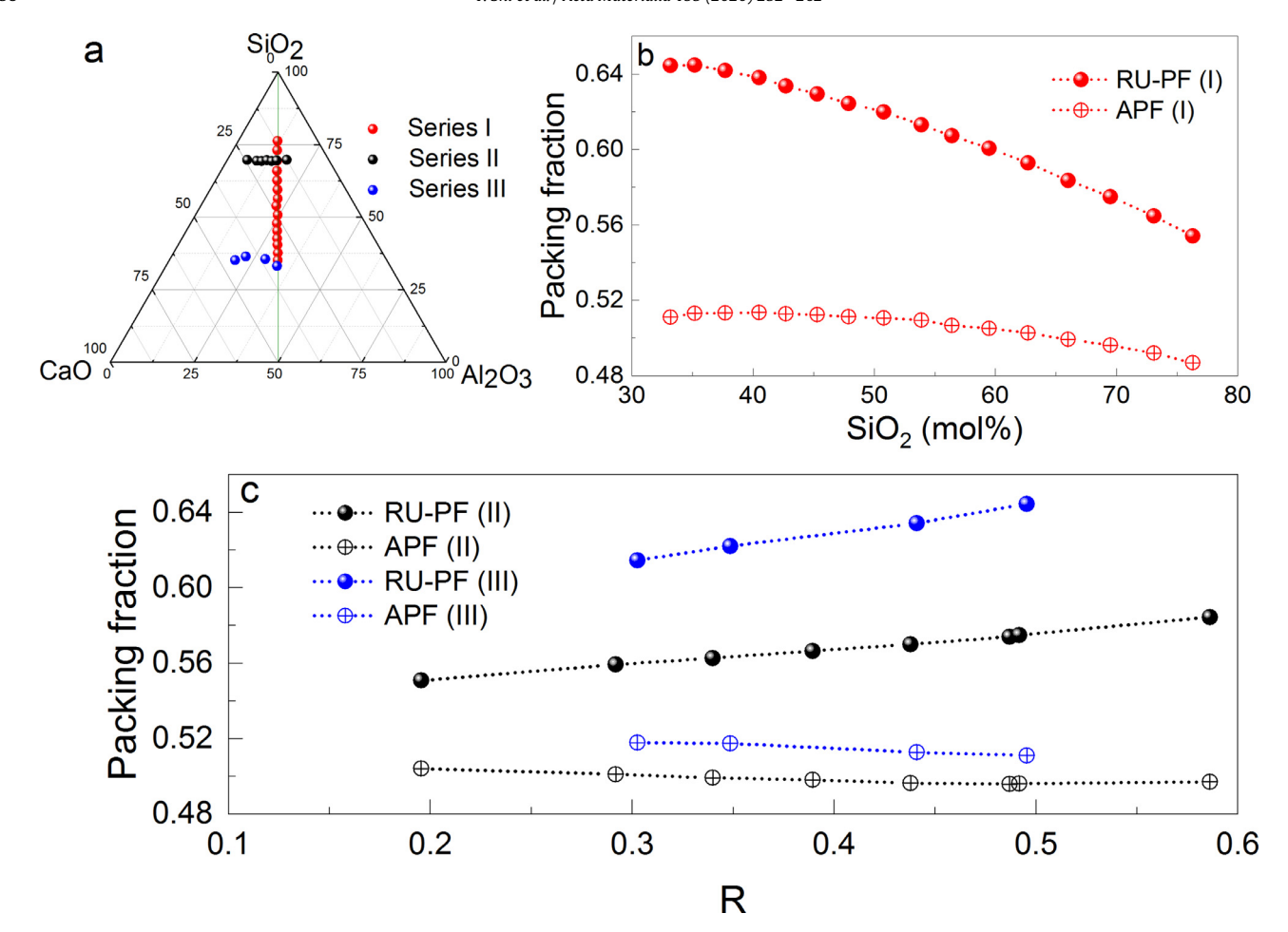


Fig. 5. Three series of CAS glasses with compositions shown in the phase diagram (a), the RUPF and APF comparison for series I charge-balanced glasses as a function of mol% of SiO₂ (red) (b), and series II (black) and III (blue) constant-SiO₂ glasses as a function of the R-value (c). (For interpretation of the references to colour in this figure legend, the reader is referred to the web version of this article.)

increased *RUPF* values which mainly originated from a high and more realistic AlO₄ tetrahedral volume compared to its *APF* value, as illustrated in Fig. 4.

3.4. Young's modulus calculated by RUPF with RUPF-derived DE

To further improve the MM-model, we now check the accuracy of the molar dissociation- energy values used for each oxide. The original G_i^{mole} values for different oxide components were computed by Sun and Huggins in 1946–47 [13,14], in which they used the molar formation energy for each oxide and the associated elemental dissociation energy from solid into uncharged gaseous atoms collected by Bichowsky and Rossini in 1936 [34]. As listed in Table 3, there are two sets of Sun-Huggins G_i^{mole} values listed for SiO₂ and Al₂O₃, but only one value for the BO₄ tetrahedral configuration, with BO₃ triangular values missing. The low G_i^{mole} value (1774 kJ/mol) for SiO₂ corresponds to fully polymerized SiO₂ where all the oxygen atoms are bridging by connecting to two Si atoms; while a high G_i^{mole} value (1950 kJ/mol) corresponds to totally depolymerized Ca₂SiO₄, where all the oxygen atoms are non-bridging oxygens which are only connected to one Si atom. The low G_i^{mole} value (2653 kJ/mol) for Al₂O₃ corresponds to aluminosilicate material; while a high G_i^{mole} value (3364 kJ/mol) corresponds to aluminate material without silicon. In the MM original paper [2], only the low G_i^{mole} value was listed for SiO_2 , while a high G_i^{mole} value was chosen for Al_2O_3 although no clear explanation and justification were provided. Interestingly, since then the MM-model users have also adjusted the G_i^{mole} values [22,23] without any physical justification.

There are no apparent reasons for us to stick to the 1940's G_i^{mole} data, as also suggested by Sun and Huggins [13] in which they stated that "the DE values computed in this paper are only approximate average values and that theoretically they should not and experimentally they do not give accurate energies of formation by simple additivity". Therefore, we decided to recalculate the G_i^{mole} values using the procedure described below.

With the new packing-fraction metric and an appropriate way to calculate *DE*, the revised MM-model is now expressed by Eq. (13)

$$E = 2\eta_{RUPF} \frac{\sum G_i^{mole} X_i}{V_m} \tag{13}$$

where η_{RUPF} is the new packing fraction, G_i^{mole} is the *DE* per mole for oxide component i, X_i is the oxide i mole fraction, and $V_{\rm m}$ is the glass' molar volume.

Eq. (13) can be rewritten as Eq. (14)

$$\frac{E}{2\eta_{RUPF}} \times V_m = \sum G_i^{mole} X_i \tag{14}$$

For 155 glasses, we would have 155 equations with 13 variables, which are the G_i^{mole} values for 11 oxides, B_2O_3 , SiO_2 , Al_2O_3 , Li_2O_3 , ... and two for Al (AlO₄ and AlO₆ with AlO₅ taking the same value as AlO₆) and two for B (BO₃ and BO₄), as listed in Table 3. A multiple linear regression with the intercept fixed at zero yields the ten refined G_i^{mole} values, which are listed in Table 3 as *RUPF*-derived DE values. The regression has an adjusted-R² value of 0.998 with an RMSE value of 1.55 kJ/mol. The errors of the calculated G_i^{mole} -values are determined by two factors: (i) the accuracy of the experimental data

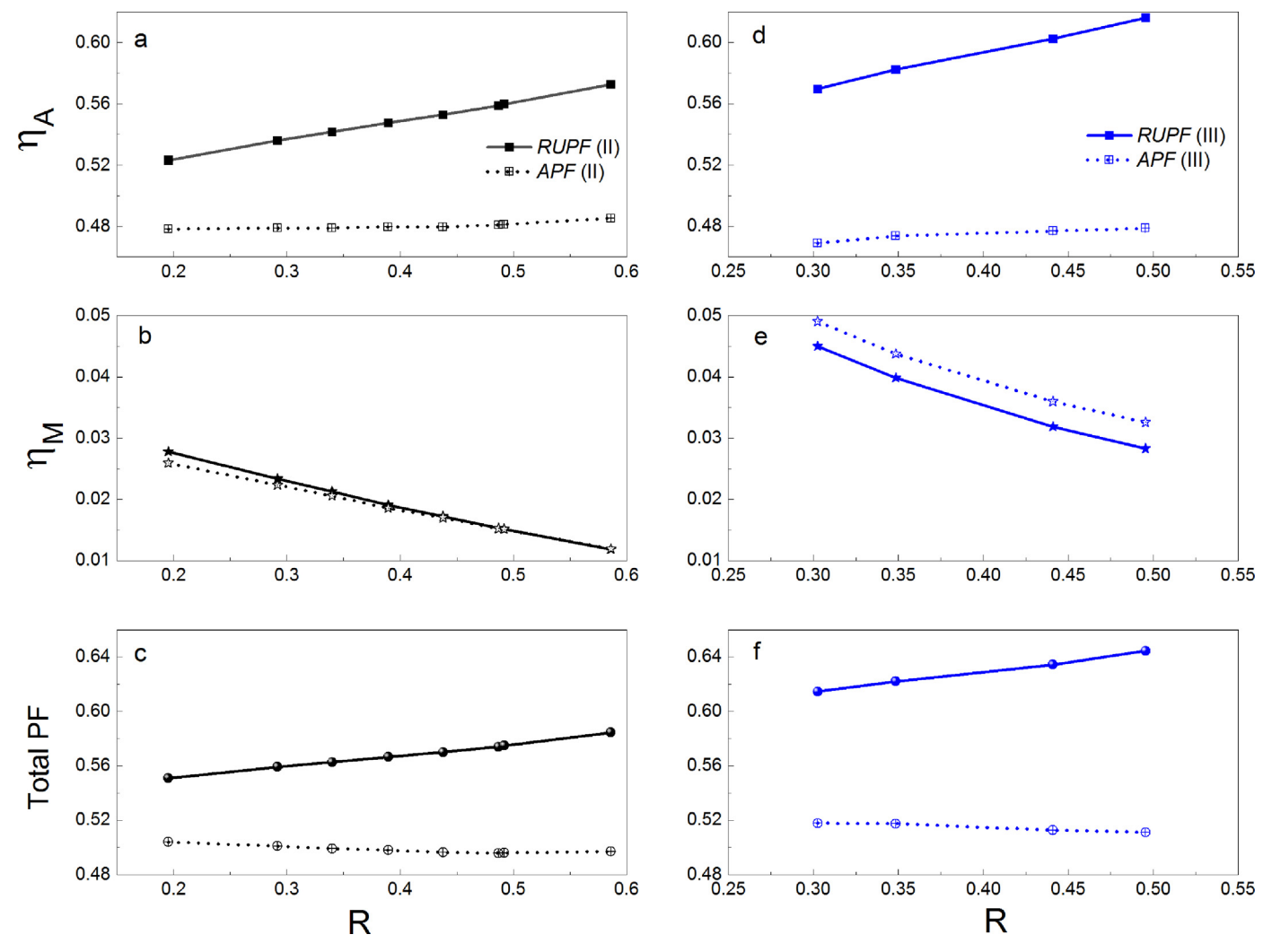


Fig. 6. Tetrahedral (η_A) , modifier (η_M) and total packing fractions as a function of *R*-value for series II (a, b & c) and III (d, e & f) CAS glasses by *RUPF* (solid) and *APF* (crossed) definitions. As the *R*-ratio increases, η_A^{RUPF} increases significantly due to the appreciably large AlO₄ vol by the *RUPF* definition, but η_A^{APF} only increases slightly with increasing Al content; both η_M^{RUPF} and η_M^{APF} decrease as the number of modifiers decreases, and for series III glasses, η_M^{RUPF} is lower than η_M^{APF} because of its smaller effective r_M deduced from the larger r_O by the high Al₂O₃ content in series III glasses; the total *RUPF* increases but *APF* slightly decreases due to its under-estimation of the tetrahedral packing fraction.

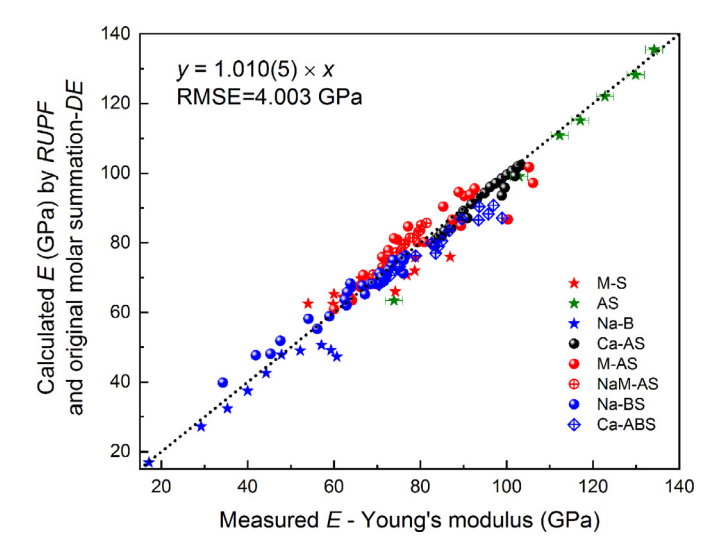


Fig. 7. Relationship between calculated and measured values of Young's modulus of 155 glasses, where the calculated value is derived by the new *RUPF* and *DE* calculated by the molar summation using original Sun values. The dotted line y = x represents the ideal correlation. The slope derived by linear fitting with the intercept fixed as zero is 1.010, and the *E*-estimation has an *RMSE* value of 4.003 GPa.

including glass composition, density and E value; and (ii) the number of glasses containing that specific oxide component. The $G_{SiO_2}^{mole}$ value has the lowest error because there are 145 glasses containing SiO₂, while the $G_{K_2O}^{mole}$ value shows the largest error because only two K₂O-containing glasses were used to derive its value.

As shown in Fig. 8, the calculated E values, derived from RUPF and RUPF-derived DE values, plotted against measured values line up very well around the ideal y = x line, with an RMSE value as low as 2.962 GPa. With such a universal set of G_i^{mole} values, the E value of glasses can be simply predicted from the sole knowledge of composition and density (or molar volume). For most glasses, the difference between calculated and measured E values is within the experimental error range of composition, density, and the E measurements. However, the deviations for non-modifier-containing aluminosilicate glasses, shown as green stars in Fig. 8, are beyond the experimental error; this might be due to the fact that the G_i^{mole} values of SiO₂ and Al₂O₃ derived from modifier-containing glasses are not applicable for glasses without modifiers, or that Al largely departs from the assumption of being in a 4-fold coordinated state. Three binary Na₂O-B₂O₃ glasses (shown as blue stars) with higher Na₂O contents $(Na_2O \text{ mol}\% \ge 40)$ also exhibit a higher deviation, which can either be due to the inaccuracy of the B coordination calculation or phase separation. In addition, we realize that the G_i^{mole} value of each oxide is

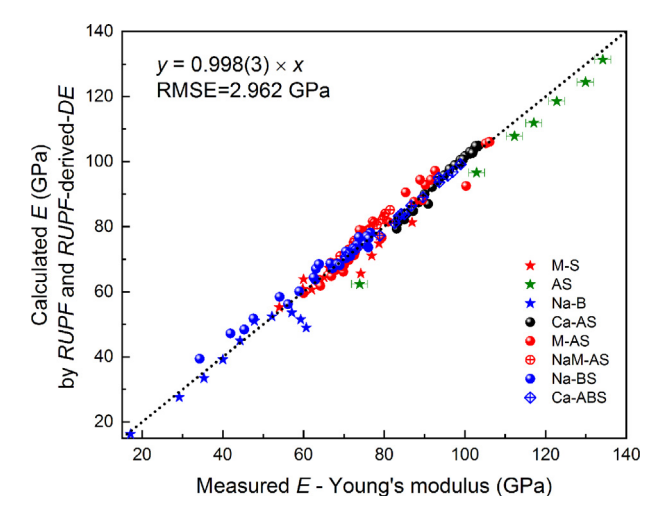


Fig. 8. Relationship between calculated and measured values of the Young's modulus of 155 glasses, where the calculated value is derived by the new *RUPF* and *RUPF*-derived G_i^{mole} -values. The dotted line y = x represents the ideal correlation. The slope derived by linear fitting with the intercept fixed as zero is 0.998, with a good *E*-estimation with an *RMSE* of 2.962 GPa.

family-dependent, that is, the Si-O bond strength in fused silica is different from that in soda-lime silicate glasses, like the two $G_{\rm SiO_2}^{mole}$ values listed in Table 3. As such, despite some limitations, our revised MM model offers an unprecedented prediction of the relationship between glass composition and Young's modulus over a large range of composition and Young's modulus values (from 15 to 140 GPa).

3.5. Young's modulus calculated by APF with APF-derived DE

To further validate our *RUPF*-derived G_i^{mole} values, we performed the same multiple linear regression using the *APF* values, as shown in Eq. (15)

$$\frac{E}{2\eta_{APF}} \times V_m = \sum G_i^{mole} X_i \tag{15}$$

Another set of 13 APF-derived G_i^{mole} values for 11 oxides are listed in Table 3. The regression has an adjusted- R^2 value of 0.998 with an RMSE value of 1.68 kJ/mol. The calculated E values calculated by APF and APF-derived DE are plotted against measured E values, as shown in Fig. 9. A similarly good E-prediction is observed, with an RMSE value of 2.954 GPa.

The four sets of DE-values derived in this study are plotted as a function of mol% of SiO_2 for CAS series I glasses in Fig. 10:1) The DE calculated by the volume summation method used in the MM paper [2] (red crossed stars); 2) the DE calculated by the correct molar summation method using the original Sun-Huggins G_i^{mole} -values [14] (blue crossed balls); 3) the DE calculated by the RUPF-derived G_i^{mole} -values (blue solid balls); 4) the DE calculated by the APF-derived G_i^{mole} -values (red solid stars). The volume summation MM-values are systematically higher than the correct molar summation values calculated from the original Sun-Huggins' data. For CAS series I glasses, our RUPF-derived data are slightly larger than the original Sun values. However, the APF-derived data are significantly larger in order to compensate the significantly lower APF values, as shown in Fig. 5(b).

Although the *APF* and *APF*-derived *DE* values yield *E* predictions with an accuracy that is similar to that achieved with *RUPF* and *RUPF*-derived *DE* values, it should be noted that a large number of fitting parameters can often yield an apparent good agreement between model and experimental data. Here, we argue that the dissociation energies obtained from the *RUPF*-based model are more realistic because they are much closer to the original values provided by Sun

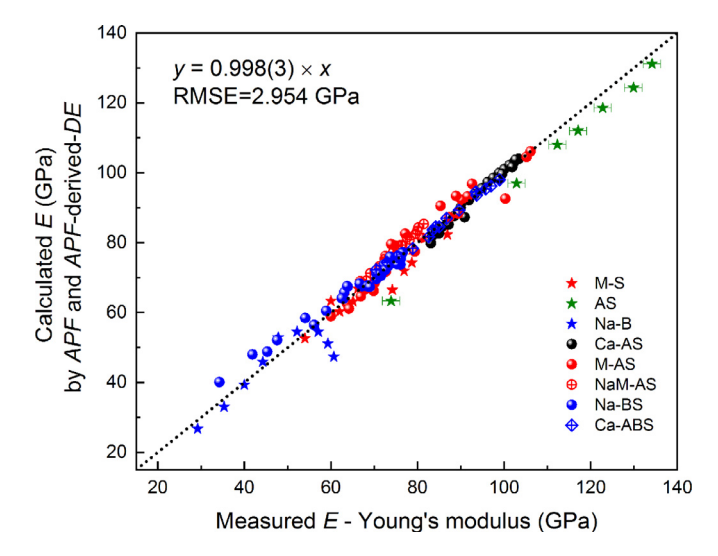


Fig. 9. Relationship between calculated and measured values of the Young's modulus of 155 glasses, where the calculated value is derived by the conventional *APF* and *APF*-derived G_i^{mole} -values. The dotted line y = x represents the ideal correlation. The slope derived by linear fitting with the intercept fixed as zero is 0.998, and a good *E*-estimation with an *RMSE* of 2.954 GPa.

[13] —as listed in Table 3, both $G_{SiO_2}^{mole}$ and $G_{Al_2O_3}^{mole}$ values for AO₄ configurations derived by *RUPF* are within the ranges computed by Sun-Huggins for different materials. In turn, the two values obtained by the *APF*-based model are significantly higher than the upper limits of the range, especially $G_{Al_2O_3}^{mole}$ obtained by *APF* is 4730 kJ/cm³, i.e., about 50% higher than the upper limit of the Sun-Huggins' value of 3364 kJ/cm³. We attribute this large discrepancy to the low *APF* value, which once again suggests that *RUPF* is a more physically-meaningful packing metric.

The *RUPF*-derived *DE* values also yield more meaningful G_i^{mole} -values for modifier oxides. As shown in Fig. 11, three types of dissociation energy (G_i^{mole}) of modifier oxides are plotted as a function of cation field strength (A^{-2}) as listed in Table 3. The cation field strength is defined as Z/r^2 with Z being the charge valence and r the Pauling effective ionic radius (also listed in Table 3). The original Sun-

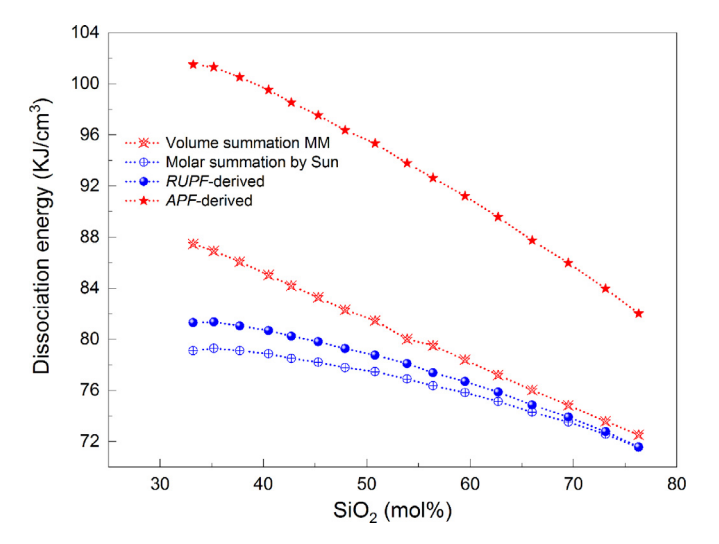


Fig. 10. Four sets of dissociation energies calculated for CAS series I charge-balanced glasses as a function of mol% of SiO₂. 1) The *DE* values calculated by the volume-summation method used in the MM-paper [2] (red crossed stars); 2) the *DE* values calculated by the correct molar-summation method using the original Sun-Huggins G_i^{mole} -values [14] (blue crossed circles); 3) the *DE* values calculated by the *RUPF*-derived G_i^{mole} -values (blue solid balls); 4) the *DE* values calculated by the *APF*-derived G_i^{mole} -values (red solid stars). (For interpretation of the references to colour in this figure legend, the reader is referred to the web version of this article.)

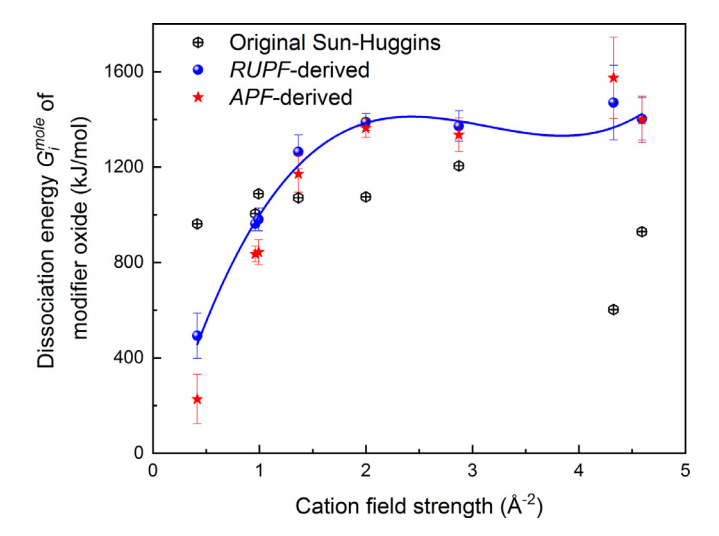


Fig. 11. Three types of dissociation energy (G_i^{mole}) of modifier oxides as a function of cation field strength (A^{-2}). The original Sun-Huggins G_i^{mole} -values [13] show no correlation with cation field strength (black crossed hexagons). Most APF-derived G_i^{mole} values (red stars) overlay with the RUPF-derived G_i^{mole} values (blue balls), but one unphysical $G_{K,O}^{mole}$ value is derived for APF with very low value. The blue line is a guide for the eye to show the correlation between RUPF-derived G_i^{mole} and the cation field strength. (For interpretation of the references to colour in this figure legend, the reader is referred to the web version of this article.)

Huggins G_i^{mole} -values [14] show no correlation with cation field strength (black crossed hexagons). Most APF-derived G_i^{mole} values (red stars) overlay with RUPF-derived G_i^{mole} values (blue balls), but an unphysical, extremely low $G_{K_2O}^{mole}$ is derived from APF—a side effect of the unphysical-high APF-based $G_{Al_2O_3}^{mole}$ value. The blue line plotted as a guide for the eye demonstrates a correlation between the RUPF-derived G_i^{mole} values and cation field strengths.

4. Conclusions

The theoretically-derived Makishima—Mackenzie (MM) model offers an intuitive physical picture to understand the relationship between glass composition and Young's modulus in terms of the inter-atomic bonding strength and the ways in which atoms are packed. We argue that the reason why it often under-estimates Young's modulus values arises from the fact that the atomic packing fraction (*APF*) defined by the MM-model notably under-estimates the packing density. Inspired by "Rigid Unit" theory, which suggests that the basic building units of a network glass should be treated as whole entities, we show that our new packing metric—the Rigid Unit packing fraction (*RUPF*)—offers a more meaningful description of the degree of packing of a glassy network. Based on this, we have shown that our revised MM model ($E = 2\eta_{RUPF} \underbrace{G_{ijmoer}^{(probet X_i)}}_{V_m}$) can predict the Young's modulus of a wide variety of oxide glasses with an unprecedented level of accuracy.

Declaration of Competing Interest

The authors declare that they have no known competing financial interests or personal relationships that could have appeared to influence the work reported in this paper.

Acknowledgements

This paper is dedicated to the memory of Prof. J. D. Mackenzie, who recently passed away. Prof. Mackenzie made countless pioneering contributions to glass and ceramics research. His beautifully simple model of glass stiffness has influenced generations of glass scientists and engineers—and we hope that the present contribution

will modestly carry on his legacy. Y.S. is grateful for the technical help and insightful discussions with Minghui Zhang and Rebecca Derosa. Thanks to Albert P. Song of Corning-Painted Post High School for figuring the geometry configuration to calculate the BO₃ interstitial space packing fraction. M.B acknowledges funding provided by the National Science Foundation under Grant 1826420.

Supplementary materials

Supplementary material associated with this article can be found in the online version at doi:10.1016/j.actamat.2020.05.047.

References

- [1] L. Wondraczek, J.C. Mauro, J. Eckert, U. Kühn, J. Horbach, J. Deubenber, T. Rouxel, Towards ultrastrong glasses, Adv. Mater. 23 (2011) 4578–4586.
- [2] A.&. Makishima, J.D. Mackenzie, Direct calculation of Young's modulus of glass, J. Non-Cryst. Solids 12 (1973) 35–45.
- [3] J.M. Mauro, A. Tandia, D. Vargheese, Y.Z. Mauro, M.M. Smedskjaer, Accelerating the design of functional glasses through modeling, Chem. Mater. 28 (2016) 4267.
- [4] K. Yang, B. Yang, X. Xu, C. Hoover, M.M. Smedskjaer, M. Bauchy, Prediction of the Young's modulus of silicate glasses by topological constraint theory, J. Non-Cryst. Solids 514 (2019) 15.
- [5] C.J. Wilkinson, Q. Zheng, L. Huang, J.C. Mauro, Topological constraint model for the elasticity of glass-forming systems, J. Non-Cryst. Solids X 2 (2019) 100019.
- [6] S. Bishnoi, S. Singh, R. Ravinder, M. Bauchy, N.N. Gosvami, H. Kodamana, N.M.A. Krishnan, Predicting Young's modulus of oxide glasses with sparse datasets using machine learning, J. Non-Cryst. Solids 524 (2019) 119643.
- [7] B. Deng, Machine learning on density and elastic property of oxide glasses driven by large dataset, J. Non-Cryst. Solids 529 (2020) 119768.
- [8] M. Plucinski, J.M. Zwanziger, Topological constraints and the Makishi-ma–Mackenzie model, J. Non-Cryst. Solids 429 (2015) 20–23.
- [9] B. Deng, J. Luo, J.T. Harris, C.M. Smith, M.E. McKenzie, Molecular dynamics simulations on fracture toughness of Al₂O₃-SiO₂ glass-ceramics, Scr. Mater. 162 (2019) 277–280.
- [10] M. Raissi, P. Perdikaris, G.E. Karniadakis, Physics-informed neural networks: a deep learning framework for solving forward and inverse problems involving nonlinear partial differential equations, J. Comp. Phys. 378 (2019) 686–707.
- [11] H. Liu, T. Zhang, N.M.A. Krishnan, M.M. Smedskjaer, J.V. Ryan, S. Gin, M. Bauchy, Predicting the dissolution kinetics of silicate glasses by topology-informed machine learning, Npj Mater. Degrad. 3 (2019) 32.
- [12] H. Liu, Z. Fu, K. Yang, X. Xu, M. Bauchy, Machine learning for glass science and engineering: a review, J. Non-Crys. Solids X 4 (2019) 100036.
- [13] M. Huggins, K.H. Sun, Energy additivity in oxygen-containing crystals and glasses, J. Phys. Chem. 50 (1946) 319–328.
- [14] K.H. Sun, M.L. Huggins, Energy additivity in oxygen-containing crystals and glasses, II, J. Phys. Colloid Chem. 51 (2) (1947) 438–443.
- [15] Y. Wang, T. Sakamaki, L.B. Skinner, Z. Jing, T. Yu, Y. Kono, C. Park, G. Shen, M.L. Rivers, S.R. Sutton, Atomistic insight into viscosity and density of silicate melts under pressure, Nat. Commun. 5 (2014) 3241.
- [16] A. Ziedler, P.S. Salmon, L.B. Skinner, Packing and the structural transformations in liquid and amorphous oxides from ambient to extreme conditions, Proc. Natl. Acad. Sci. USA 111 (28) (2014) 10045–10048.
- [17] J. Wu, T.M. Gross, L. HUang, S.P. Jaccani, R.E. Youngman, S.J. Rzoska, M. Bockowski, S. Bista, J.F. Stebbins, M.M. Smedskjaer, Composition and pressure effects on the structure, elastice properties and hardness of aluminosilicates glass, J. Non-Cryst. Solids 530 (2020) 119797.
- [18] Y.H. Yun, P.J. Bray, Nuclear magnetic resonance studies of the glasses in the system Na₂O-B₂O₃-SiO₂, J. Non-crystal. Solids 27 (1978) 363–380.
- [19] A. Osaka, Network Structure of Binary and Ternary Glasses Based on Additivity Rule. Okayama University Ph.D. Thesis. 1984.
- [20] L.M. Thompson, J.F. Stebbins, Non-bridging oxygen and high-coordinated aluminum in metaluminous and peraluminous calcium and potassium aluminosilicate glasses: high-resolution ¹⁷O and ²⁷Al MAS NMR results, Am. Mineral. 96 (2011) 841–853.
- [21] S. Inaba, S. Fujino, K. Morinaga, Young's modulus and compositional parameters of oxide glasses, J. Am. Ceram. Soc. 82 (12) (1999) 3501–3507.
- [22] S. Inaba, S. Todaka, Y. Ohta, K. Morinaga, Equation for estimating the Young's modulus, shear modulus and Vickers hardness of aluminosilicate glasses, J. Japan Inst. Metals 64 (3) (2000) 177–183.
- [23] S. Inaba, S. Oda, K. Morinaga, Equation for estimating the thermal diffusivity, specific heat and thermal conductivity of oxide glasses, J. Japan Inst. Metals 65 (8) (2001) 680–687.
- [24] G.A. Rosales-Sosa, A. Masuno, Y. Higo, H. Inoue, Crack-resistant Al₂O₃—SiO₂ glasses, Sci. Rep. 6 (2016) 23620.
- [25] A. Ponitzsch, M. Nofz, L. Wondraczek, J. Denbener, Bulk elastic properties, hardness and fatigue of calcium aluminosilicate glasses in the intermediate-silica range, J. Non-Cryst. Solids 434 (2016) 1–12.
- [26] C. Weigel, C. Le Losq, R. Vialla, C. Dupas, S. Clement, D.R. Neuville, B. Ruffle, Elastic moduli of XAlSiO₄ aluminosilicate glasses: effects of charge-balancing cations, J. Non-Cryst, Solids 447 (2016) 267–272.

- [27] M. Ren, J. Cheng, S.P. Jaccani, S. Kapoor, R.E. Youngman, L. Huang, J. Du, A. Goeal, Composition – structure – property relationships in alkali aluminosilicate glasses: a combined experimental – computational approach towards designing functional glasses, J. Non-Cryst. Solids 505 (2019) 144–153.
- [28] M.M. Smedskjaer, J.C. Mauro, J. Kjeldsen, Y. Yue, Microscopic origins of compositional trends in aluminosilicate glass properties, J. Am. Ceram. Soc. 96 (5) (2013) 1436–1443.
- [29] L. Pauling, Nature of chemical bond and structure of molecules and crystals, Cornell University Press, Ithaca, N.Y., 1940.
- [30] J.W. E. Whittaker, R. Muntus, Ionic radii for use in geochemistry, Geochim. Cosmochim. Acta 34 (9) (1970) 945–956.
- [31] J.H. Conway, N.J.A. Sloane, Sphere Packings, Lattices, and Groups, Springer-Verlag, New York, 1993.
- [32] M. Grehn, T. Seuthe, M. Hofner, N. Griga, C. Theiss, A. Mermillod-Blondin, M. Eberstein, H. Eichler, J. Bonse, Femtosecond-laser induced ablation of silicate glasses and the intrinsic dissociation energy, Opt. Mater. Express 4 (4) (2014) 689–700.
- [33] M.T. Dove, K.D. Hammonds, M.J. Harris, V. Heine, D.A. Keen, A.K.A. Pryde, K.O. Trachenko, M.C. Warren, Amorphous silica from the rigid unit mode approach, Mineral. Mag. 64 (2000) 377–388.
- [34] F.R. Bichowsky, F.D. Rossini, The Thermochemistry of the Chemical Substances (1936).